Magnon coherent conductance via atomic nanocontacts

2007 J. Phys.: Condens. Matter 19 266208

(http://iopscience.iop.org/0953-8984/19/26/266208)

IOP PUBLISHING JOURNAL OF PHYSICS: CONDENSED MATTER

J. Phys.: Condens. Matter **19** (2007) 266208 (12pp) doi:10.1088/0953-8984/19/26/266208

Magnon coherent conductance via atomic nanocontacts

B Bourahla[1,2,4], **A Khater**[1,4], **R Tigrine**[1,2], **O Rafil**[2] **and M Abou Ghantous**[3]

[1] Laboratoire de Physique de l'Etat Condensé UMR 6087, Université du Maine, 72085 Le Mans, France
[2] Laboratoire de Physique et Chimie Quantique, Université Mouloud Mammeri, 15000 Tizi-Ouzou, Algeria
[3] School of Sciences, Lebanese American University, PO Box 36 Byblos, Lebanon

E-mail: bourahla_boualem@yahoo.fr and antoine.khater@univ-lemans.fr

Received 25 March 2007, in final form 9 May 2007
Published 7 June 2007
Online at stacks.iop.org/JPhysCM/19/266208

Abstract

A calculation for the coherent scattering and conductance of magnons via atomic nanocontacts is presented. The model system is composed of two groups of semi-infinite magnetically ordered Heisenberg monatomic chains, joined together by the magnetic nanocontact, and the system is supported on a non-magnetic substrate and considered otherwise free from magnetic interactions. The coherent transmission and reflection coefficients are derived as elements of a Landauer-type scattering matrix. Transmission and reflection scattering cross sections are calculated specifically for three distinct symmetric and asymmetric geometric configurations of the nanocontact. Three cases of local magnetic exchange on the nanocontact domain are analysed for each configuration to investigate the influence of softening and hardening of the magnetic boundary conditions. In analogy with coherent electronic transport, we calculate the magnon coherent transport. The numerical results show the interference effects between the incident scattered magnons and the localized spin states on the nanocontact, with characteristic Fano resonances. The numerical results yield an understanding of the relationship between the coherent magnon conductance and the architecture of the embedded magnetic nanocontact.

(Some figures in this article are in colour only in the electronic version)

1. Introduction

It is possible, using modern techniques, to prepare well-defined nanostructures as constitutive elements of mesoscopic systems. These are of technological interest in a variety of devices. The study of nanostructures in general, and *at surfaces* in particular, has been the subject of major research efforts in recent years. There is, consequently, an increasing volume of experimental

[4] Authors to whom any correspondence should be addressed.

0953-8984/07/266208+12$30.00

data and findings to elucidate the structural [1–4], magnetic [5–7], and electronic [8–11] properties of finite quasi-one-dimensional (1D) nanostructures and monoatomic chains on surfaces.

Scattering and localization phenomena in low-dimensional systems have also been of interest for a long time. They are now of renewed interest in the context of the nanometric devices. Most of the recent research in this area has been oriented towards the study of electronic scattering in quasi-1D systems. The understanding of electronic transport in the mesoscopic regime and its generalization to multi-terminal systems has been provided by the formalism of Landauer [12], and Büttiker [13], who related the system conductance to its scattering matrix.

Multiple scattering and quantum interference are not limited, however, to the sole area of electronic transport. In a variety of problems they can become important, and describe the coherent transport phenomena via nanostructures embedded in low-dimensional systems [14–17]. Because of the relevance of spin dynamics in certain devices for information processing, the problem of localized magnons, in particular [18], and of magnon transport has received some attention recently. At low temperatures, these devices are mesoscopic in the sense that their quantum states must be described by coherent wavefunctions extending over the entire system, and quantum-mechanical interference effects become important [19]. This has been illustrated recently for spin currents in mesoscopic Heisenberg systems [20].

The purpose of this work is to present a model for the study of coherent magnon transport via atomic nanocontacts. These are considered to act as magnetic joints between two groups of semi-infinite magnetically ordered monatomic chains. The system is supported on a non-magnetic substrate, and considered otherwise free from magnetic interactions. This model does not consider thermal effects [20], effects related to lead connections [21], or inelastic scattering effects due to some additional internal degrees of freedom of the nanostructure [22]. The purpose here is to give a basic understanding for the relation between the coherent magnon conductance via the nanocontact, and the structural configuration of the latter.

The paper is organized as follows. In section 2 we present the basic elements of the model, describing the spin dynamics on the group of monatomic chains which constitute an effective quasi-1D waveguide, on either side of the nanocontact domain. In section 3 we study the spin dynamics of the nanocontact itself. The transmission and reflection scattering cross sections are then derived, using the matching method [23–26]. In section 4 numerical applications are presented for three different configurations of the nanocontact domain. The first corresponds to a perfectly symmetric single-atomic nanocontact, the second to an asymmetric single-atomic nanocontact, and the third to an asymmetric multi-atomic nanocontact. For each of these configurations we analyse the magnon conductance under three different boundary conditions as regards the local magnetic exchange on the nanocontact domain. The numerical application of the model and the scattering results and conclusions are presented in this section.

2. Basic elements of the model

The models studied in this paper for the magnon conductance via nanocontacts are presented successively in figures 2(a), 3(a), and 4(a). These three lattice systems have in common two identical groups of triple parallel semi-infinite monatomic chains as input and output quasi-1D waveguides. The chains are considered ferromagnetically ordered with no loss of generality, their spins being normal to the plane of the chains. For ferromagnetic Heisenberg exchange between nearest neighbours, the Hamiltonian of the ground state is given by

$$H = -2 \sum_{p \neq p'} J_{pp'} \mathbf{S}_p \cdot \mathbf{S}_{p'}. \tag{1}$$

$\mathbf{S}_p$ ($\mathbf{S}_{p'}$) are the spin vectors, where $p \equiv n, m$ are integers that run along the x and y directions, respectively. The spins are assumed to be ordered along the direction normal to the plane of the monatomic chains. The exchange constants $J_{pp'} = J$ coupling the magnetically nearest-neighbour sites in the system are the same everywhere except on the nanocontact domain. This is delimited as a shaded rectangular domain in figures 2(a), 3(a), and 4(a), for which $J_{pp'} = J_d$ identifies an exchange constant for the atoms, which may be different from the rest of the system.

The three cases analysed for each nanocontact are characterized by the following boundary possibilities, for $\gamma = J_d/J$, namely

$$\gamma = J_d/J < 1, \qquad \gamma = J_d/J = 1, \qquad \gamma = J_d/J > 1. \tag{2}$$

For $\gamma < 1$ and $\gamma > 1$, a magnetic softening or hardening is said to take place on the nanocontact. For $\gamma = 1$ the exchange is the same throughout the system. We assume that $J_{pp'}$ for the nanocontact may be prepared by the insertion of a different type of ion than that for the rest of the system, or that $J_{pp'}$ may be modified and tuned by technical means. It is also assumed that the exchange is homogeneous on the sites of the nanocontact domain.

The method employed to study the spin dynamics may be described by the equations of motion for the spin precessions on atomic sites p; see [18] for details. Consider the spin precessions $\zeta_p^{\pm}(t) = \zeta_{px}(t) \pm \mathrm{i}\zeta_{py}(t)$, where $\zeta_{p\alpha}(t) = S_{p\alpha}(t) - \langle S_{p\alpha} \rangle$, the brackets are thermal averages, and α denotes the Cartesian directions; $\alpha = z$ is normal to the substrate.

In the matching procedure [25], used to calculate the magnon properties for our system, each kind of magnon symmetry is studied separately. A secular equation is first derived which is shown to contain in particular all the information on the dispersion curves and density of states of the chain magnons along the reciprocal-space direction not contained in the subspace associated with the nanocontact domain. The spin precession states of the nanocontact domain and the resonances are obtained within a single framework by matching the evanescent and travelling solutions, respectively, of the secular equation, satisfying the boundary conditions brought about by the nanocontact. A localized nanocontact spin precession state is found to be the sum of evanescent spin states on the chains. The magnons of the same frequency travelling to and away from the nanocontact are related to one another by reflection coefficients, for which sum rules are derived.

For chain sites p distant from the nanocontact boundaries, $n \leqslant -2$ and $n \geqslant 2$, the system of equations for the spin dynamics to the left and right of the shaded domains in figures 2(a), 3(a), and 4(a) may be cast in the form

$$[\Omega \boldsymbol{I} - D(\eta)]|\zeta_p^{\pm}\rangle = 0. \tag{3}$$

$\Omega = \omega/\omega_0 = \hbar\omega/2JS$ is a dimensionless frequency for the bulk of the magnetic chains, where $S = |\mathbf{S}_p| \cdot \boldsymbol{I}$ denotes a unit matrix, and $D(\eta)$ is a spin dynamics matrix characteristic of the perfect group of magnetic chains. η is a generic phase factor between neighbouring sites on the chains along the x direction. In this representation, $|\zeta_p^{\pm}\rangle$ is the corresponding vector of the spin precessions for a unit cell of magnetically ordered triple parallel magnetic monatomic chains. The matrix $[\Omega \boldsymbol{I} - D(\eta)]$ is an irreducible form for the three inequivalent sites per unit cell. Both the propagating and the evanescent eigenmodes are described by the phase factor doublets $\{\eta, \eta^{-1}\}$.

The propagating magnon modes are determined by the condition that $|\eta_x| \equiv |\exp(\mathrm{i}\phi_x)| = 1$, whereas the evanescent modes are determined from the condition $|\eta_x| < 1$ [23, 26]. The exact solutions for each doublet are obtained as a function of the frequencies Ω. These solutions are obtained when the secular equation of the spin dynamic matrix $[\Omega \boldsymbol{I} - D(\eta)]$ vanishes. For the system under study the secular equation may be expressed as a polynomial of

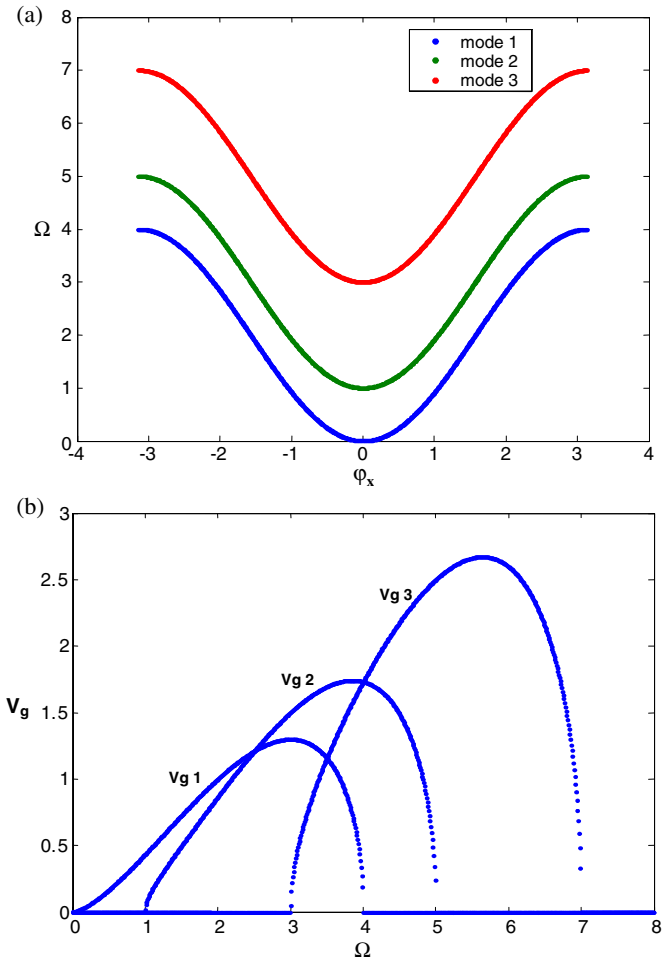

Figure 1. (a) The magnon dispersion curves on a quasi-1D crystalline waveguide made from triple parallel semi-infinite monatomic chains, coupled magnetically with ferromagnetic order normal to the plane of the chains in the $\Omega \in [0, 7]$ interval. (b) The group velocities of the magnon modes in this interval.

degree six in η_x:

$$\sum A_s(\Omega)\eta_x^s = 0. \tag{4}$$

$A_s(\Omega)$ are the polynomial coefficients. Due to the Hermitian nature of the spin dynamics in the absence of strong external magnetic fields, both phase factors $\{\eta_x, \eta_x^{-1}\}$ verify the polynomial forms symmetrically.

The solutions of equation (4) provide the eigenmodes of the system. There are, however, only three modes of physical interest. For the propagating modes η_{xi}, their inverse η_{xi}^{-1} are modes propagating in the opposite sense, both representing magnon dispersion. For the non-propagating modes, only the evanescent modes $|\eta_{xi}| < 1$ are considered, their inverse representing non-physical divergent modes.

The magnons for the perfect chain waveguides and their group velocities are given in figure 1. Their dispersion branches are presented as a function of the normalized wavevector

$\phi_x = k_x a$, where a is the lattice parameter, and ϕ_x runs over the first Brillouin zone in the interval $[-\pi, \pi]$.

3. Nanocontact spin dynamics and scattering

To analyse the scattering in the presence of an embedded nanostructure, such as those presented in figures 2(a), 3(a), and 4(a), it is essential to know the evanescent $|\eta_{xi}| < 1$, as well as the propagating solutions $|\eta_{xi}| = 1$, for a complete description of the scattering processes. Since the perfect chain waveguides do not couple between different eigenmodes, we can treat the scattering problem for each eigenmode separately.

For a magnon mode η_{xi}, incident at a frequency Ω from the left to the right along the x direction, the elastic scattering outputs due to the nanocontact are coherent reflected and transmitted fields. Let R_{ij} and T_{ij} denote the reflection and transmission coefficients that describe the scattering. For sites in the waveguide to the right and the left of the nanocontact, the spin precession field $\{\zeta_p^{\pm}\}$, where $n \leqslant -2$ and $n \geqslant 2$, may be expressed in terms of an appropriate superposition of the eigenmodes of the perfect waveguide at the same frequency. Consider a Hilbert space constructed from the basis vectors $[|\boldsymbol{R}\rangle, |\boldsymbol{T}\rangle]$ for the reflection and transmission into the different eigenmodes, and let $|\zeta_p^{\pm}(\text{nano})\rangle$ group the spin precessions for an irreducible set of spins in the nanocontact domain, $n \in [-1, +1]$. The equations of motion for this domain, coupled to the rest of the system, may be written in terms of the vector $[|\zeta_p^{\pm}(\text{nano})\rangle, |\boldsymbol{R}\rangle, |\boldsymbol{T}\rangle]$. Use of the transformations connecting the spin precession field, in the matching approach, yields a square linear inhomogeneous system of equations of the form

$$[\Omega \boldsymbol{I} - D(\{\eta_{xj}\}, \gamma)][|\zeta_p^{\pm}(\text{nano})\rangle, |\boldsymbol{R}\rangle, |\boldsymbol{T}\rangle] = -|\boldsymbol{IH}, \eta_{xi}\rangle \tag{5}$$

where the vector $-|\boldsymbol{IH}, \eta_{xi}\rangle$, mapped appropriately onto the basis vectors in the constructed Hilbert space, regroups the inhomogeneous terms describing the incoming magnon.

In scattering phenomena, the reflection and transmission effects are described in terms of the scattering matrix elements [12, 13], which are given explicitly by the reflection coefficient R_{ij} for the backward scattered or reflected waves j, and the transmission coefficient T_{ij} for the forward scattered or transmitted wave j, per incident propagating mode i.

The scattering behaviour for the magnons is described, as for the coherent scattering of other excitations, in terms of the scattering matrix. For different incident magnons i, the solutions of equation (5) yield the reflection and transmission coefficients R_{ij} and T_{ij} on the perfect waveguides, and the spin precession vector $|\zeta_p^{\pm}(\text{nano})\rangle$ for the irreducible set of spins on the nanocontact domain. The reflection and transmission scattering cross sections r_{ij} and t_{ij} are then given at the scattering frequency Ω as

$$\begin{aligned} r_{ij} &= (v_{gj}/v_{gi})|R_{ij}|^2 \\ t_{ij} &= (v_{gj}/v_{gi})|T_{ij}|^2. \end{aligned} \tag{6}$$

The scattering cross sections are normalized with respect to the group velocities of the magnons to obtain unitarity for the scattering matrix. v_{gi} is the group velocity of the eigenmode i; it is equal to zero for evanescent modes. The group velocities of the magnon modes on the group of triple parallel monatomic chains in the waveguide are presented in figure 1(b).

We can define total reflection and transmission cross sections for a given eigenmode i at frequency Ω by summing over all the contributions of the scattered magnons:

$$\begin{aligned} r_i(\Omega) &= \sum_j r_{ij}(\Omega) \\ t_i(\Omega) &= \sum_j t_{ij}(\Omega). \end{aligned} \tag{7}$$

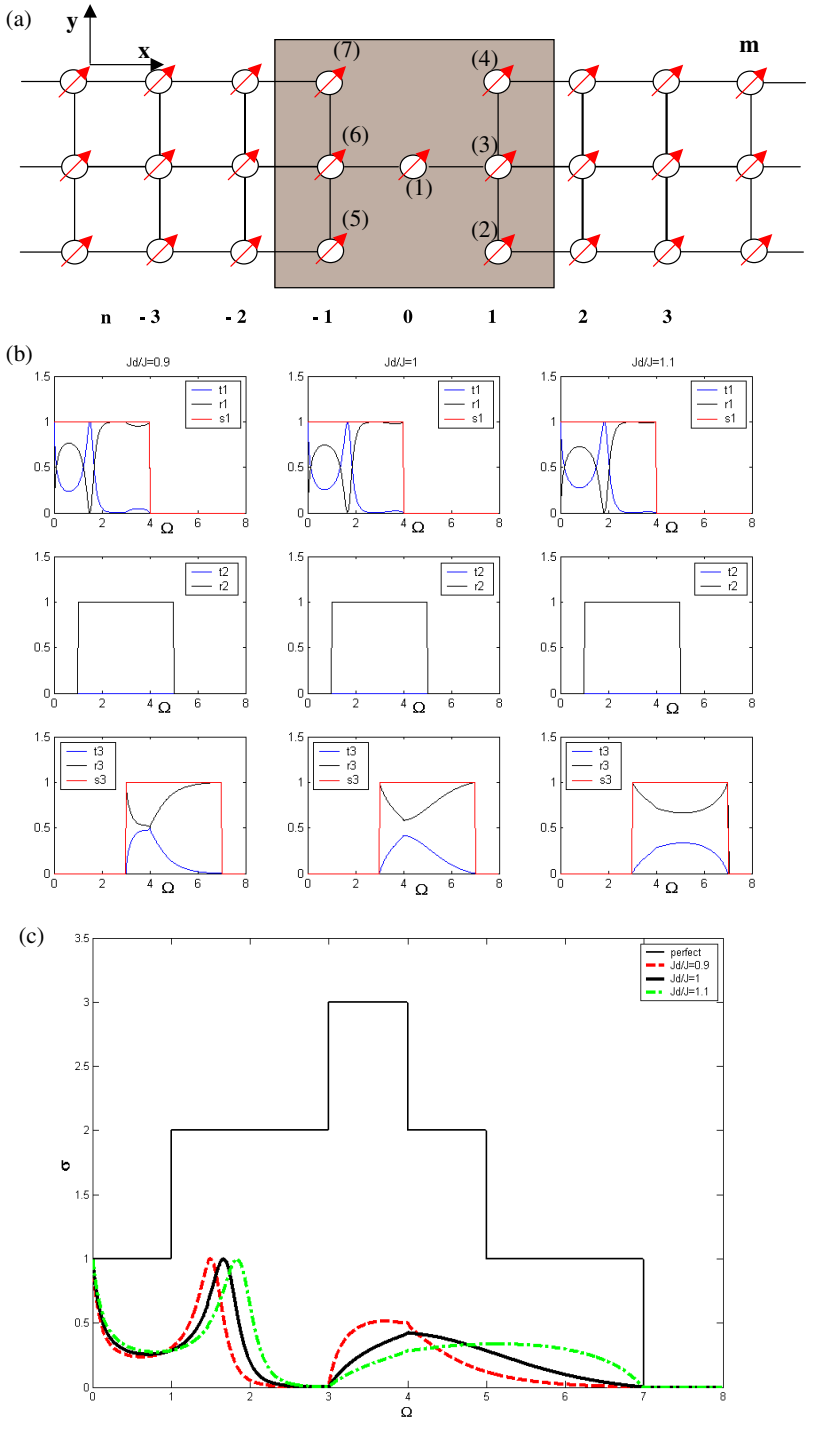

Figure 2. (a) A schematic representation of the quasi-1D crystalline waveguide with a perfectly symmetric atomic nanocontact configuration. The nanocontact domain is the shaded rectangle. (b) The reflection and transmission cross sections for the magnon modes, for the (a) configuration. See text for details. (c) The calculated total magnon conductance $\sigma(\Omega)$ in $\Omega \in [0, 7]$, for the (a) configuration.

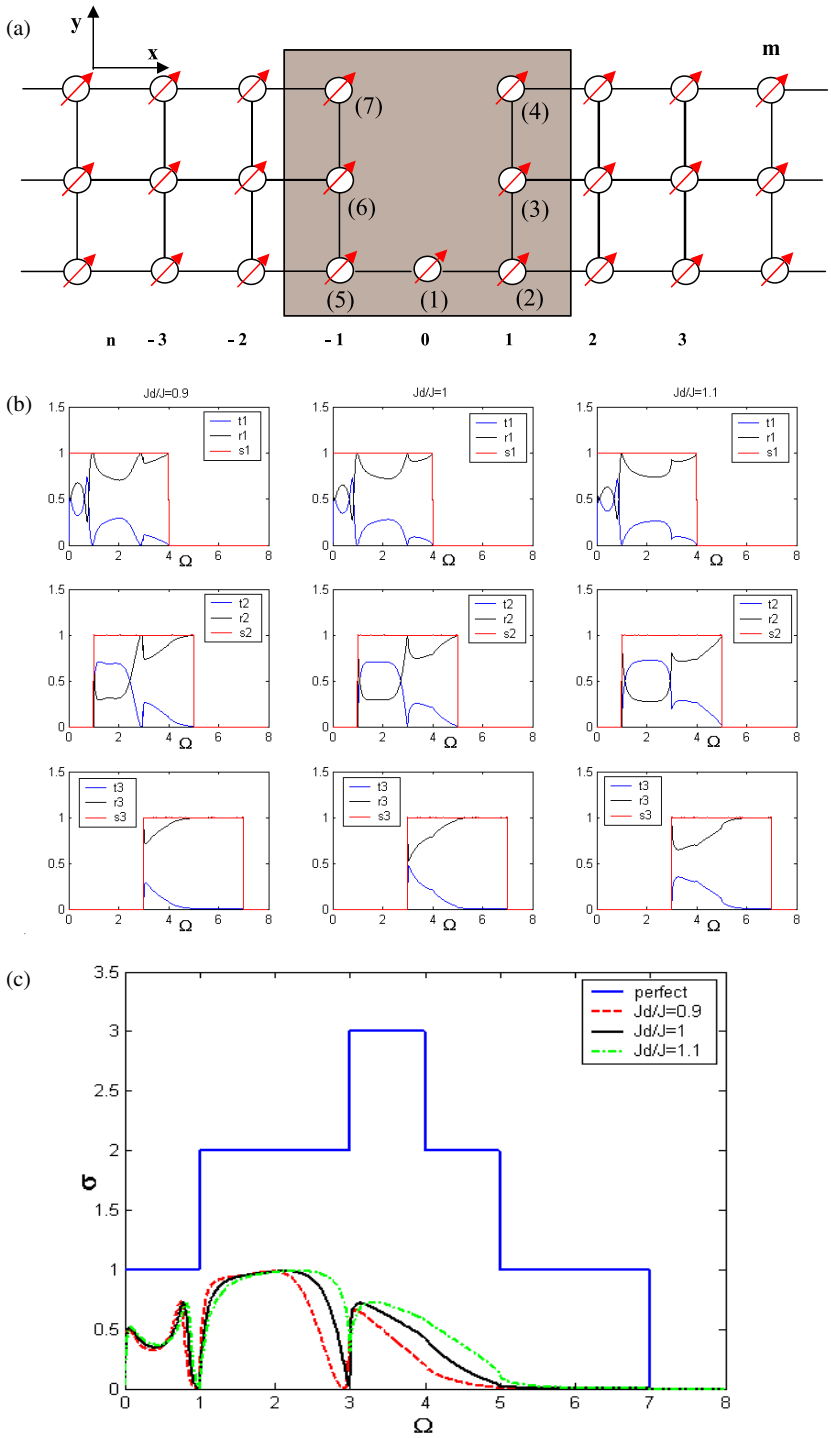

Figure 3. (a) As in figure 2(a), for an asymmetric atomic nanocontact. (b) and (c) As figures 2(b) and (c), respectively, here for the (a) configuration.

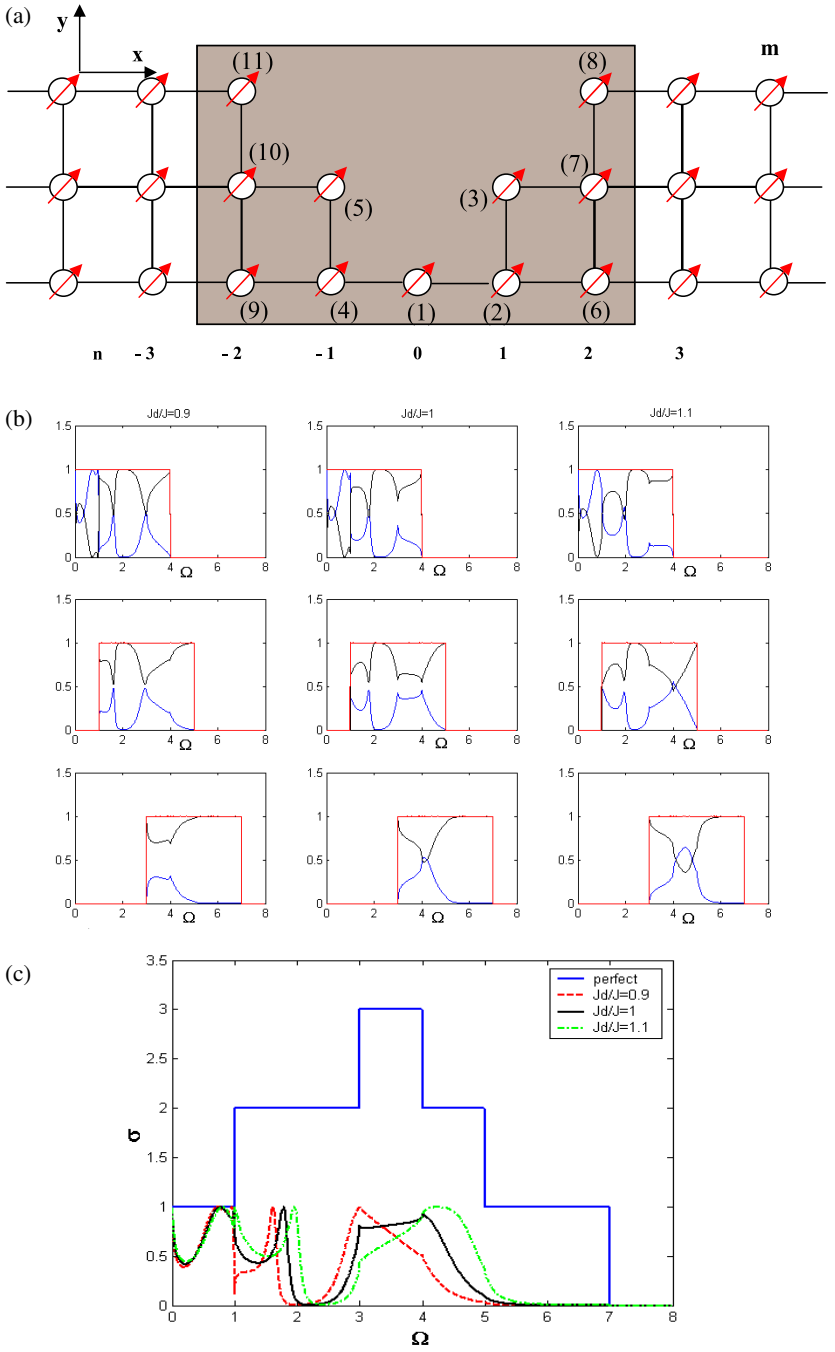

Figure 4. (a) As in figure 2(a), for an asymmetric multi-atomic nanocontact configuration. (b) and (c) As in figures 2(b) and (c), respectively, here for the (a) configuration.

Furthermore, in order to describe the overall transmission of a mesoscopic multi-channel system at a given frequency Ω, it is useful to define the total magnon conductance, or

nanostructure transmittance, $\sigma(\Omega)$:

$$\sigma(\Omega) = \sum_i \sum_j t_{ij}(\Omega), \tag{8}$$

where the sum is carried out over all input and output channels at the frequency Ω. The transmission scattering cross section, $t_i(\Omega)$, per incident magnon i, and the conductance of the system, $\sigma(\Omega)$, are important quantities to calculate. Although it is probably not very clear which observables could really be measured in a real magnon transport experiment, these calculated quantities are nevertheless basic to a full understanding of the magnon transport measurements.

4. Numerical applications and discussion

In figure 1 the dispersion branches for the magnons of the perfect waveguides are presented over the first Brillouin zone in the interval $[-\pi, \pi]$. The magnons labelled $i \in \{1, 2, 3\}$, from bottom to top in that order, are propagating modes in the respective frequency intervals

$$\begin{aligned} \Omega_1 &= [0, \Omega_{1,\max} = 4] \\ \Omega_2 &= [1, \Omega_{2,\max} = 5] \\ \Omega_3 &= [3, \Omega_{3,\max} = 7]. \end{aligned} \tag{9}$$

The eigenmodes of the waveguide are either symmetric or antisymmetric with respect to the central axis in the x direction. Symmetric modes correspond to spin precession displacements that satisfy the conditions

$$\zeta^{\pm}_{n,m} = \zeta^{\mp}_{n,M+1-m} \tag{10}$$

whereas for the antisymmetric modes they satisfy

$$\zeta^{\pm}_{n,m} = -\zeta^{\mp}_{n,M+1-m}. \tag{11}$$

M is the total number of chains along the y direction. There is one acoustic mode, Ω_1, characterized by its limiting behaviour, which tends to zero frequency when ϕ_x tends to zero, and two optical modes with branches that differ from zero in the long-wavelength limit.

Our numerical results do not address any particular experiment. Nevertheless, it is interesting to note that the experimental systems at present which are most relevant for the theoretical study of magnon transport presented in this paper would probably be the magnetic break junctions and magnetic point contacts [27–31].

The results of the numerical applications of our scattering model are presented for three different geometric configurations of the nanocontact domain. For each configuration we analyse the magnon conductance under three different boundary conditions as regards the local magnetic exchange on the nanocontact domain, compared to that for the bulk of the atomic chains. The three possibilities analysed are for $\gamma = 0.9$, 1.0 and 1.1 respectively. For $\gamma < 1$ (> 1), a magnetic softening (hardening) is said to take place on the nanocontact domain. For $\gamma = 1$, the local exchange is the same as throughout the system. The contact configurations, and the numerical results for their magnon conductance properties, are grouped in figures 2–4, respectively.

The numerical results for the first nanocontact configuration of a single symmetric atomic contact are presented in figure 2. The nanostructure configuration itself is presented schematically in figure 2(a), where the atomic joint is placed symmetrically in the system. Figure 2(b) presents the reflection and transmission cross sections for the three magnon modes. These are arranged in rows for the variation in magnetic exchange in the naocontact domain, from softening at the left to hardening at the right, and in rows per magnon mode, ranging from

mode 1 at the top to mode 3 at the bottom. The transmission and reflection cross sections verify the unitarity condition for the scattering matrix, and this is used throughout as a check on the numerical calculation. For each case, we present for comparison the transmission histogram per magnon mode for the perfect quasi-1D waveguide. Furthermore, figure 2(c) presents the total magnon conductance, $\sigma(\Omega)$, in $\Omega \in [0, 7]$, the total interval for the propagation of the magnons; their transmission on the perfect quasi-1D waveguide is presented in the form of a global histogram for reference.

In a similar manner, the corresponding numerical scattering results for the two other nanocontact configurations, namely the asymmetric single-atomic contact and the asymmetric multi-atomic contact, are presented in figures 3 and 4, respectively.

The results show some general characteristics, as well as some specific magnon behaviour, for each of the three contact configurations.

The total magnon conductance, $\sigma(\Omega)$, is less than or equal to one magnon throughout the $\Omega \in [0, 7]$ interval, for all three configurations. This illustrates how the single-atomic nanocontact at the heart of the contact domain in each case constricts the transmission to a maximum of one magnon at a time, which is characteristic for the single-atomic chain $n \in [-1, +1]$.

Another general characteristic of the total magnon conductance is the displacement of its spectral features to higher frequencies with increasing hardening of the magnetic exchange in the nanocontact domain, for all three configurations, which is a signature of the nanocontact matching necessary for the transmission.

Some of the spectral maxima in the interval $\Omega \in [0, 7]$ correspond to characteristic Fano resonances, since the spin precession states on the nanocontact domain are effectively localized states embedded in the continuum of the waveguide incident magnon modes. See [32] for a detailed discussion of the Fano resonance. These localized states are dynamic spin states for which the spin precession field decreases in amplitude with distance from the nanocontact domain into the chains, in conformity with the evanescent modes on the chains. Their energies displace, naturally, to higher frequencies with increasing magnetic exchange in the nanocontact domain.

The other maxima of the spectral features correspond, however, to the variation in the magnon conductance between the pinning minima which are imposed by the limits of the propagating intervals of the magnon modes. These limits may be readily understood from figure 1(b), which gives the group velocities of the magnon modes over their propagating intervals. Note that the transmission histogram per magnon mode for the perfect quasi-1D waveguide is also a useful reference to these intervals, as in figures 2(c), 3(c), and 4(c).

In particular, for the first, and symmetric, atomic contact, the features of the conductance spectrum attributed to Fano resonances, Ω_F, correspond to the maxima that shift through the frequencies $\Omega_F = 1.50$, 1.66, and 1.85, with increasing $\gamma = 0.9$, 1.0, and 1.1, as in figure 2(c). Comparing figures 2(b) and (c), we observe that it is the mode 1 magnons which effectively contribute these Fano resonances in the total conductance spectrum. In contrast, the mode 2 magnons have a particular behaviour, as they fail to be transmitted and are completely reflected in their entire propagation interval. Technically, we may say that the perfectly symmetric atomic contact filters out these asymmetric optic mode 2 magnons, as they do not couple to the symmetric localized spin precession states. Furthermore, the mode 2 magnons do not couple, on the nanocontact domain, to the two other magnon modes 1 and 3, which leads to a conductance spectrum that is relatively well defined over the propagating intervals of modes 1 and 3. The sharp features close to $\Omega = 3$ and 4, and to 7, in figure 2(c), correspond hence to the critical behaviour of the magnon modes 1 and 3 at the limits of their propagating intervals. The broad features in the interval [3, 7], which shift to higher frequencies with increasing γ,

do not correspond to Fano resonances, and are partially pinned at $\Omega = 4$ due to the interaction of mode 3 with mode 1 magnons on the nanocontact domain. The broad features in the total conductance spectrum correspond effectively to the transmission spectra of mode 3 magnons.

Note that mode 3, a high-energy optic mode, shows no Fano resonance for any of the contact configurations. It is partially transmitted in its propagating interval for the symmetric atomic nanocontact, and is completely filtered out in the $\Omega \in [5,\ 7]$ interval, for the asymmetric nanocontact configurations.

For the second, and asymmetric, atomic nanocontact, the features of the conductance spectrum attributed to Fano resonances, Ω_F, correspond to the maxima that shift through the frequencies $\Omega_F = 0.70$, 0.74, and 0.78, with increasing $\gamma = 0.9$, 1.0, and 1.1, as in figure 3(c). Such resonances, similar in form to those in figure 2(c), are again due to the interaction of the continuum of mode 1 magnons with the localized spin precession states. Interestingly, however, the localized states are at frequencies that are roughly half of those for the symmetric atomic nanocontact. Their reduced values may hence be attributed to the reduction of the ensemble of magnetic interactions on the asymmetric nanocontact, in comparison with those on the symmetric nanocontact. The broad features in the intervals [1, 3] and [3, 7], as in figure 3(c), which shift to higher frequencies with increasing γ, do not correspond to Fano resonances. These features are pinned at $\Omega = 3$ and 4, due to the interactions of mode 2 magnons, with mode 3 and mode 1 magnons respectively, on the nanocontact domain. Note that the pinning is partially lifted at $\Omega = 3$ and 4 with increasing γ (see details in rows one and two of figure 3(b)). This confirms the non-Fano character of the broad features. The sharp features close to $\Omega = 1$ and 3 correspond to the critical behaviour of the magnon modes 2 and 3 at the limits of their propagating intervals.

Finally, for the third, and asymmetric, multi-atomic nanocontact, the features of the conductance spectrum attributed to Fano resonances, Ω_F, are the maxima that shift through the frequencies 1.64, 1.82, and 2.0, with increasing $\gamma = 0.9$, 1.0, and 1.1, as in figure 4(c). These Fano resonances correspond to localized spin precession states that are different from those for the symmetric single-atomic contact. Furthermore, although the symmetry-breaking effect appears similar for nanocontacts in figures 3 and 4, the conductance spectrum changes drastically. Absent from the symmetric atomic nanocontact (for symmetry considerations), and also absent from the asymmetric single-atomic contact (because the localized spin precession states lie energetically below its propagating interval), the mode 2 magnons interact at present with the characteristic localized spin states in the asymmetric multi-atomic contact to produce Fano resonances. These resonances, as may be observed in figure 4(b), are hence due to the interaction of the continuum of mode 1 magnons, as well as that of mode 2 magnons, with the localized spin precession states. In contrast, the broad features in the interval [$\sim$2.5, $\sim$5.5], do not correspond to Fano resonances. The sharp features in this interval correspond again to the pinning at $\Omega = 3$ and 4, partially lifted with increasing γ.

An interesting observation is the relatively important total magnon conductance, $\sigma(\Omega)$, across the perfectly symmetric single-atomic nanocontact in the interval $\Omega \in [5,\ 7]$, when the other two modes cease to exist as propagating modes. In contrast, $\sigma(\Omega)$ suffers total reflection, and is technically filtered out completely by the asymmetric nanocontacts in this frequency interval. It is hence likely that the third magnon mode is symmetric optic.

In conclusion, we present a model to calculate the scattering properties of magnons and their coherent transport via atomic nanocontacts. The purpose is to give an understanding of the relation between the coherent magnon conductance via these contacts and their symmetry properties. The nanocontacts are considered to act as magnetic joints between two groups of semi-infinite magnetically ordered monatomic chains, with Heisenberg interactions. Finally, it is also interesting to note, in recent references concerning the magnetic break junctions [27, 28],

that some of their properties are driven by resonant states that are localized in the junction domain.

Acknowledgments

AK would like to thank A R P Rau for useful correspondence, and RT and BB would like to thank the University of Tizi Ouzou for financial support and the Université du Maine for their study visit.

References

[1] Shchukin V and Bimberg D 1999 *Rev. Mod. Phys.* **71** 1125
[2] Gambardella B, Blanc M, Burgi L, Kuhnke K and Kern K 2000 *Surf. Sci.* **449** 93
[3] Kern K, Niehaus H, Schatz A, Zeppenfeld P, Goerge J and Comsa G 1991 *Phys. Rev. Lett.* **67** 855
[4] Rousset S *et al* 2002 *Mater. Sci. Eng.* B **96** 169
[5] Gambardella P, Dallmeyer A, Maiti K, Malagoli M C, Rusponi S, Ohresser P, Eberhardt W, Carbone C and Kern K 2004 *Phys. Rev. Lett.* **93** 077203
[6] Vindigni A, Rettori A, Pini M G, Carbone C and Gambardella P 2006 *Appl. Phys.* A **82** 385
[7] Weiss N, Cren T, Epple M, Rusponi S, Baudot G, Tejeda A, Repain V, Rousset S, Ohresser P, Scheurer F, Bencok P and Brune H 2005 *Phys. Rev. Lett.* **95** 157204
[8] Crain J N and Pierce D T 2005 *Science* **7** 703
[9] Bürgi L, Jeandupeux O, Hirstein A, Brune H and Kern K 1998 *Phys. Rev. Lett.* **81** 5370
[10] Hasegawa Y and Avouris P 1993 *Phys. Rev. Lett.* **71** 1071
[11] Repp J, Meyer G and Rieder K H 2004 *Phys. Rev. Lett.* **92** 036803
[12] Landauer R 1957 *IBM J. Res. Dev.* **1** 223
Landauer R 1970 *Phil. Mag.* **21** 863
[13] Büttiker M 1986 *Phys. Rev. Lett.* **57** 1761
[14] Tekman E and Bagwell P F 1993 *Phys. Rev.* B **48** 2553
[15] Berthod C, Gagel F and Maschke K 1994 *Phys. Rev.* B **50** 18299
[16] Fellay A, Gagel F, Maschke K, Virlouvet A and Khater A 1997 *Phys. Rev.* B **55** 1707
[17] Belhadi M, Khater A, Rafil O, Hardy J and Tigrine R 2001 *Phys. Status Solidi* b **228** 685
[18] Khater A and Abou Ghantous M 2002 *Surf. Sci. Lett.* **498** L97
[19] Imry Y 1997 *Introduction to Mesoscopic Physics* (Oxford: Oxford University Press)
[20] Schütz F, Kollar M and Kopietz P 2003 *Phys. Rev. Lett.* **91** 017205
[21] Dhar1 A and Shastry B S 2003 *Phys. Rev.* B **67** 195405
[22] Imry Y, Entin-Wohlman O and Aharony A 2005 *Europhys. Lett.* **72** 263
[23] Abou Ghantous M and Khater A 1999 *Eur. Phys. J.* B **12** 335
[24] Feuchtwang T E 1967 *Phys. Rev.* **155** 731
[25] Szeftel J and Khater A 1987 *J. Phys. C: Solid State Phys.* **20** 4725
[26] Belhadi M, Rafil O, Tigrine R, Khater A, Hardy J, Virlouvet A and Maschke K 2000 *Eur. Phys. J.* B **15** 435
[27] Chantis A N, Belashchenko K D, Tsymbal E Y and van Schilfgaarde M 2007 *Phys. Rev. Lett.* **98** 046601
[28] Burton J D, Sabirianov R F, Velev J P, Mryasov O N and Tsymbal E Y 2007 at press
(Burton J D, Sabirianov R F, Velev J P, Mryasov O N and Tsymbal E Y 2007 *Preprint* cond-mat/0703345)
[29] Bolotin K I, Kuemmeth F, Pasupathy A N and Ralph D C 2006 *Nano Lett.* **6** 123
[30] Khvalkovskii A V, Zvezdin K A and Zvezdin A K 2005 *Microelectron. Eng.* **81** 336
[31] Viret M *et al* 2002 *Phys. Rev.* B **66** 220401
[32] Fano U 1961 *Phys. Rev.* **124** 1866
Rau A R P 2004 *Phys. Scr.* **69** 1